

Optimization of the Diode-Pumped Solid State Nd:YLF Amplifier Chain for the 263 nm Drive Laser at the FAST Facility

Julie M. Gillis

*Department of Physics
Department of Chemistry and Biochemistry
Bayer School of Natural and Environmental Science
Duquesne University
Pittsburgh, PA 15282*

James K. Santucci and Jinhao Ruan

*Fermilab Accelerator Science and Technology (FAST) Facility
Accelerator Division
Fermi National Accelerator Laboratory
Batavia, IL 60510*

Summer Internships in Science and Technology (SIST) Program
August 6, 2015
Fermi National Accelerator Laboratory



Table of Contents

Contents.....	2
Abstract.....	3
Introduction.....	4
Fermi National Accelerator Laboratory	
FAST Research	
<i>Superconducting Accelerator Research</i>	
<i>Integrable Optics Test Accelerator</i>	
FAST Laser Lab	
<i>Drive Laser System</i>	
<i>Solid State Amplifier Chain</i>	
Background.....	8
Laser Principles	
<i>Stimulated Emission</i>	
Optical Amplifiers	
<i>Diode End-Pumped Amplifiers</i>	
<i>Nd:YLF as a Gain Medium</i>	
<i>Nd:YLF Energy Levels and Transitions</i>	
Electron Bunches	
<i>The Photoelectric Effect</i>	
<i>Photocathodes</i>	
SIST Project Description.....	14
Methods.....	15
Instrumentation	
<i>Laser Probe Inc. Rm-3700 Universal Radiometer</i>	
<i>Thorlabs DET10A Si Biased Detector</i>	
<i>Agilent Technologies DSO6104A Digital Storage Oscilloscope</i>	
<i>Prosilica GC 2450 CCD Camera</i>	
Drive Laser Schematic	
<i>Seed Pulse Pick-Off</i>	
Nd:YLF Amplifier Schematic	
Data and Results.....	18
Preliminary Measurements	
<i>Pump Diode Characterization</i>	
<i>Single-Pass Amplifier 3 (SPA3)</i>	
<i>Test Single-Pass Amplifier (SPAT)</i>	
Timing Adjustments	
Alignment Work	
<i>Maximization of SPAT Gain</i>	
Switching SPAT and SPA3	
<i>Diagnostic Diode Calibration</i>	
Downstream Results of New Amplifier	
<i>Effects on Northrop Grumman Amplifier (NGA)</i>	
<i>Effects on Ultraviolet Pulse Energy</i>	
Conclusions.....	27
Future Work.....	28
Acknowledgements.....	29
References.....	30

Abstract

The RF photoinjector of the 50 MeV superconducting electron linear accelerator at the Fermilab Accelerator Science and Technology (FAST) Facility is driven by a phase-locked laser system. The YLF seed laser provides short (3 ps) infrared (1053 nm) pulses to an amplifier chain before conversion to ultraviolet (263 nm) through two frequency-doubling BBO crystals. The amplification section consists of seven diode-pumped solid state (DPSS) amplifiers, which increase the pulse energy of the seed laser by optically end pumping neodymium-doped yttrium-lithium fluoride (Nd:YLF) crystals with 808 nm laser diodes. To maximize the total gain of the amplifier chain, each stage must be properly tuned with optimized optics, alignment, and laser beam characterization. In this paper we report on one of the single-pass amplifier improvements to achieve a consistent gain of 4.83 with stabilized output pulse trains for up to 1500 seed pulses. The ultraviolet pulses imaged onto the Cs₂Te photocathode of the RF electron gun have been doubled in energy to 10.2 μJ per pulse as a result of these alterations.

Introduction

Fermi National Accelerator Laboratory

Founded in 1967, Fermi National Accelerator Laboratory is the United States' premier particle physics laboratory. The lab, funded by the Office of Science of the Department of Energy, is situated on a 6800-acre site in Batavia, Illinois, approximately forty miles west of the city of Chicago. Known for the 28 year legacy of the Tevatron, the world's highest-energy proton-antiproton collider, Fermilab boasts the discovery of the top quark, the tau neutrino, five B baryons, and the observation of direct CP violation in kaons, along with many other achievements [23].

Following the mission of the laboratory's first director, Robert R. Wilson, the lab continues to search for answers to the mysteries of matter, energy, space, and time for not only the scientific community, but the global community as well. Today, Fermilab is the world leader in neutrino research with the LBNF/DUNE, NOvA, and MicroBooNE experiments [24]. Fermilab is also dedicated to muon experiments, the dark-matter and dark-energy searches, and advanced accelerator technology development.

FAST Research

The Fermilab Accelerator Science and Technology (FAST) Facility is home to the only active electron beamline at Fermi National Accelerator Laboratory. As an advanced accelerator research and development (AARD) facility, FAST is a testbed for numerous innovative accelerator design

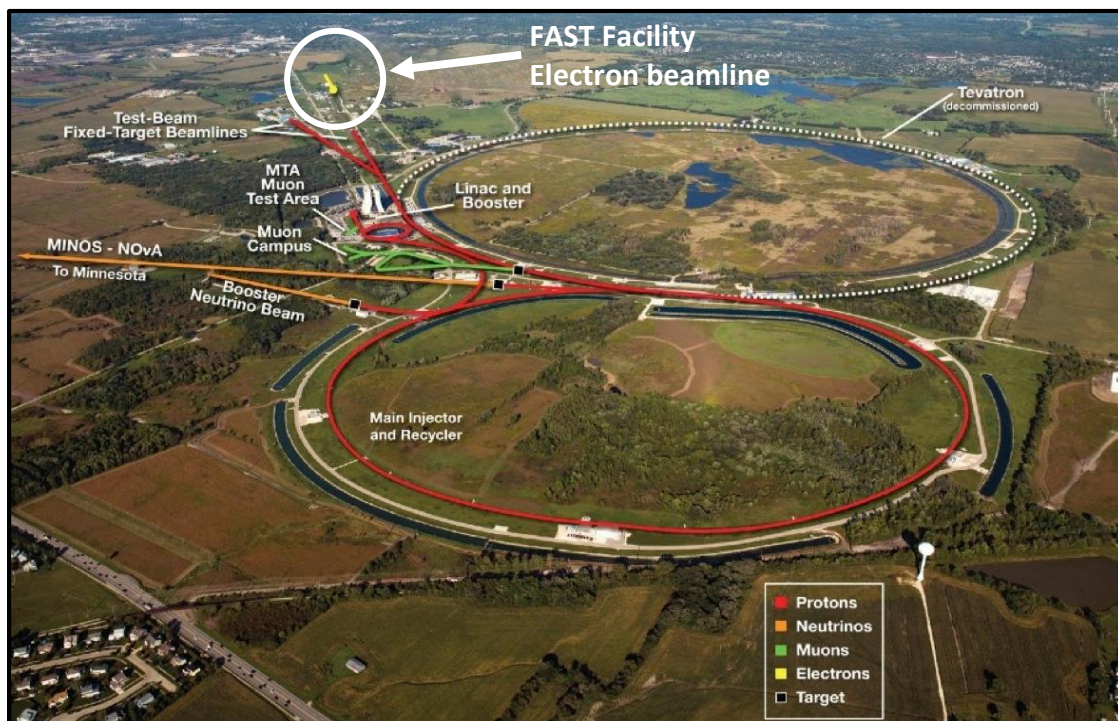


Figure 1. An aerial view of the accelerator complex at Fermi National Accelerator Laboratory and the operating beamlines as of 2015. FAST Facility and its 50 MeV electron beam are located at the north end of the laboratory complex. Adapted from [25].

technologies and diagnostic elements. In particular, FAST focuses on superconducting accelerator design and nonlinear, integrable accelerator optics for the Intensity and Energy Frontiers of high-energy particle physics.

Superconducting Accelerator Research

The accelerator at FAST consists of a superconducting radiofrequency (SRF) linear accelerator coupled to a photoinjector. Electron bunches with energies of approximately 5 MeV are produced by an RF electron gun at the upstream end of the beamline. The electron beam is accelerated to 50 MeV at its low-energy end by two capture cavities (CC1 and CC2). Both of these contain a nine-cell niobium cavity operating at a resonant frequency of 1.3 GHz [1]. Each cavity is welded into a helium vessel for super-cooling with cryogenic liquids to reach the desired operating temperature of 1.7 K [2].

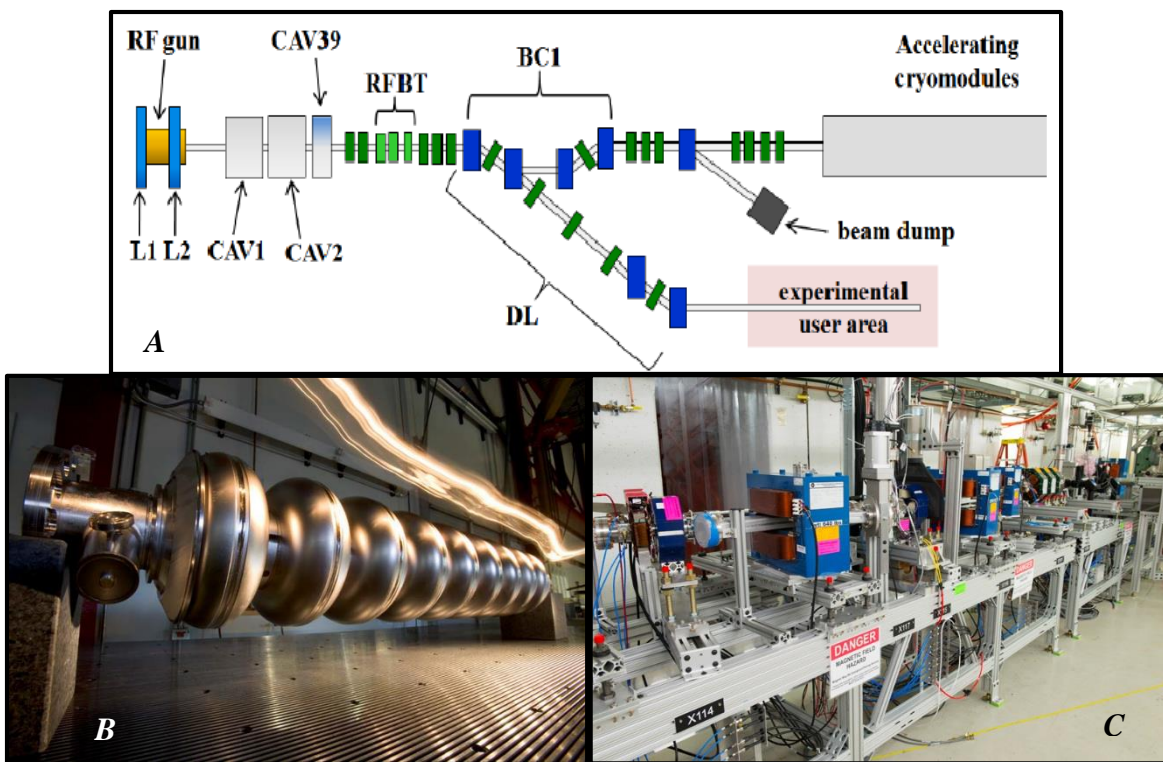


Figure 2. A) Schematic of the photoinjector and low-energy end of the electron beamline at FAST. [1] B) A photo of a bare nine-cell niobium SRF cavity. [30]. C) Bending dipole magnets and focusing quadrupole magnets along the beamline inside the FAST enclosure. [30].

Downstream of the two accelerating cavities, a series of quadrupole and dipole magnets, for focusing and bending respectively, is used to achieve optimal beam parameters. Various diagnostic elements, such as transverse profile monitors, are used throughout the beamline to characterize the electron beam in real time and make corrections before it reaches the low-energy beam dump. Future plans will allow the beam to reach energies of 300 MeV once the enclosure and beamline are extended to the high-energy beam dump by connecting a Tesla Test Facility (TTF)/ILC-type cryomodule containing a string of eight nine-cell SRF cavities [1]. The high-energy end of the beam will be used to test an innovative nonlinear lattice design for circular accelerators.

Integrable Optics Test Accelerator

To address intensity limitations of typical accelerator designs, a small storage ring will be coupled to the downstream, high-energy end of the beamline for ring-based AARD. The Integrable Optics Test Accelerator (IOTA) ring currently under construction at FAST will have a circumference of 39 meters and will store electrons of energies up to 150 MeV [2]. After commissioning of IOTA is completed with electrons, the ring will store high-energy protons for further circular accelerator studies.

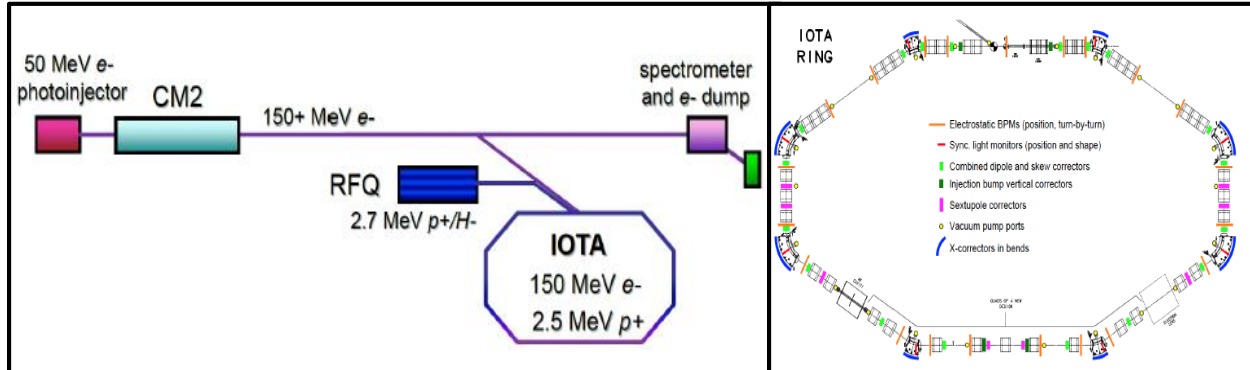


Figure 3. Schematic of the Integrable Optics Test Accelerator (IOTA) ring design for testing nonlinear lattices in circular accelerators. Adopted from [26].

All current accelerators are designed with linear focusing optics, or lattices, which are typically responsible for intensity-limiting aspects of the accelerators, such as machine resonances, tune shifts, and other instabilities [2]. By implementing a nonlinear lattice in the IOTA ring, progress can be made toward alleviating limitations on the intensity of particle accelerator beams. IOTA will consist of several integrable optics segments with highly nonlinear magnets. With successful testing of the IOTA design, circular particle accelerators will hold more tightly focused beams containing a larger number of particles, resulting in a higher number of collisions and more data for analysis.

FAST Laser Lab

The photoinjector drive laser system for the superconducting accelerator at FAST is contained in an 8.7 m x 6.5 m room adjacent to the upstream end of the beam enclosure [1]. The temperature and humidity controlled laser room holds three optical tables. The main optical table contains the photocathode drive laser system, and the two remaining tables are used for laser R&D. A vacuum pipe runs from the laser lab to the beam tunnel to transport the ultraviolet laser pulses to the photocathode of the RF electron gun.

Drive Laser System

The photocathode drive laser system at FAST is based on the A0 photoinjector used at Fermilab's A0 Lab for R&D. Upgrades to the original A0 design have been made including the use of Nd:YLF crystals rather than Nd:glass as the amplifier gain medium and the implementation of pulsed diodes to pump the medium in place of flash lamps [1].

The seed laser operates at 1.3 GHz and creates ultrashort pulses of 1053 nm (IR) light with a pulse width of 3 picoseconds. Using a Pockels cell, or pulse picker, small bunches of pulses are selected

from the seed laser-produced pulses with the correct timing for use in the pre-amplifiers and solid-state amplifier chain. The amplified infrared pulses then pass through a series of two BBO (barium borate) frequency-doubling crystals to generate the fourth harmonic wavelength of the seed laser's 1053 nm light [3]. The first doubling crystal induces 526.5 nm (green) light and the second doubling crystal creates the desired 263.25 nm (ultraviolet) pulses that are used in the photocathode of the RF electron gun to create the electron beam.

Solid State Amplifier Chain

In order for the drive laser system to be optimally efficient as a source of electromagnetic radiation to create electron bunches from the photocathode of the RF electron gun, the energy of the light pulses must be increased. By breaking up the amplifier into various stages, a larger gain can be obtained, thus producing higher energy pulses. The seed pulse is amplified at 1053 nm, before reaching the frequency-doubling crystals and generating the fourth harmonic wavelength. The amplifier chain in the FAST laser lab consists of three pre-amplifiers and three single-pass solid state amplifiers in series, followed by a commercial amplifier. These amplifiers are end-pumped using two near-infrared laser diodes with a wavelength of 808 nm [3]. The gain medium used in these amplifiers is a neodymium-doped yttrium-lithium fluoride (Nd:YLF) crystal.

Background

Laser Principles

The word “laser” is an acronym for the method by which the device operates: *light amplification by stimulated emission of radiation* [4]. Typically, a lasing medium is contained within an optical cavity and is able to emit photons with a specific energy and wavelength. The lasing medium must be pumped with energy in order to create a population inversion of the electrons stored within the medium. Population inversion occurs when there are more atoms in a metastable, excited energy state than in the ground state. As some of the electrons begin to spontaneously decay to lower energy levels, they release photons which interact with other atoms and cause the same decays to occur. This results in a chain reaction of stimulated decays of photons with the same wavelength, phase, and direction [5]. Because this laser process occurs within the optical cavity, usually consisting of a long tube with mirrors at either end, a fraction of the photons are reflected back and forth between the mirrors, allowing the beam to be amplified as more stimulated emission occurs with each pass of photons through the lasing medium. Eventually, when the signal is strong enough, the beam is able to pass through one of the end mirrors, which is partially transparent, to produce a usable laser beam.

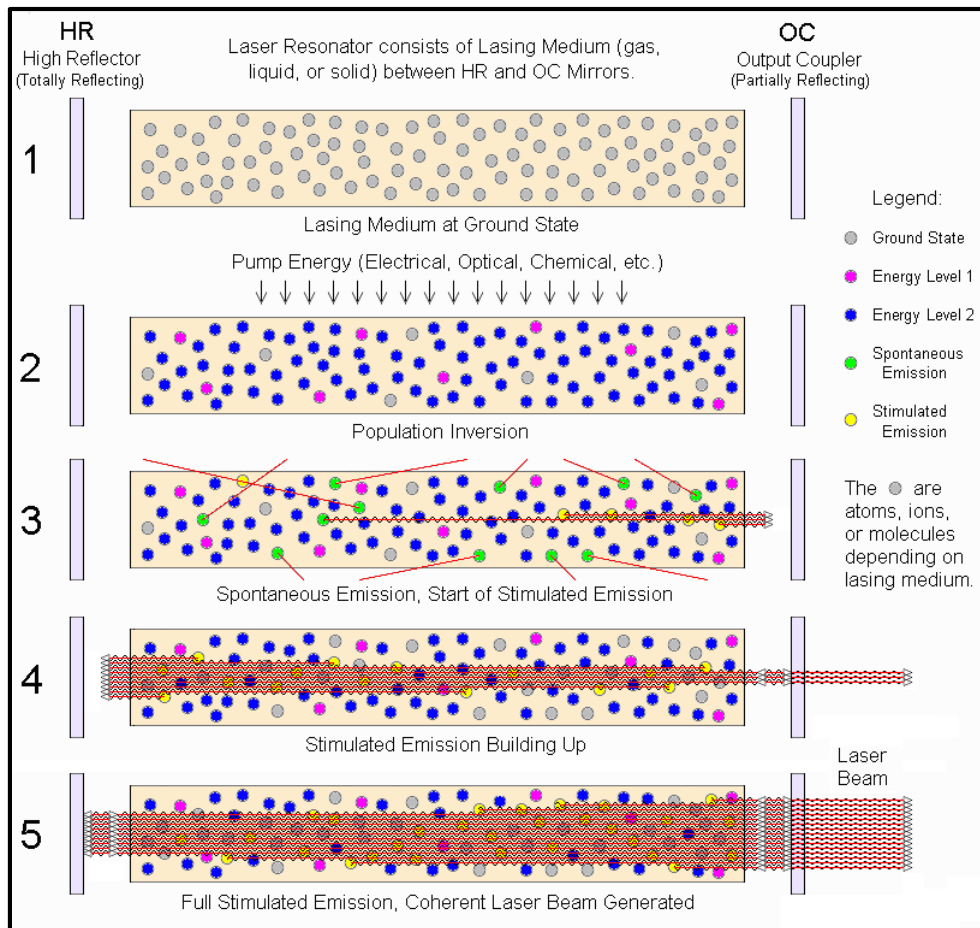


Figure 4. Diagram showing the five key steps of basic laser operation within the optical cavity which lead to the stimulated emission of coherent, monochromatic, and collimated laser light. Adopted from [27].

The light emitted by a laser differs from that of a normal light source in three essential ways that make laser beams useful for scientific and technological applications. A laser beam is described as a coherent, monochromatic, and collimated light source [5]. Coherence refers to the property of laser light that is a direct result of stimulated emission. Because the same incident light induces the decay of all of the excited atoms, the photons released have a phase relationship, exhibiting both temporal and spatial coherence. The monochromatic property of a laser refers to the tendency of the source of the light to come from a single atomic transition, resulting in a light beam with a single wavelength. This causes the laser light to have only one spectral color, even if it is not a visible light wavelength. As a result of the Doppler effect on the moving atoms, the spectral emission line still has a finite width, and is therefore not exactly monochromatic [4]. Despite this fact, lasers still provide the purest and most widely-accessible source of monochromatic light. Laser beams are also collimated, meaning they can propagate along a large distance without diverging drastically. The typically small beam radius of laser light and its tight focus contribute to their strong irradiance and output power.

Stimulated Emission

When laser-active atoms are excited out of their ground state into a higher quantum energy level, they have absorbed energy from an external source, usually in the form of a photon. Eventually, these excited atoms will drop back to a more stable, lower energy level. This can happen via the process of spontaneous emission, resulting in the ejection of a photon with energy proportional to the atomic transition and in a random spatial direction. In contrast, stimulated emission processes utilize an incident beam of light which causes the excited atom to decay into a lower energy state. The photons released as a result of the atom's change in energy are not randomly released, rather they fall into the same spatial direction as the stimulating signal [5]. Stimulated emission is a key process, not only for basic laser operation, but also in optical amplifiers.

Optical Amplifiers

To effectively amplify an optical signal, producing an output energy or power greater than that of the input signal, various techniques have been developed each with their own merits depending on the application. Optical amplifiers are able to produce gain in an optical signal without having to first convert it to an electrical signal. Some of the most widely used types of optical amplifiers include doped-fiber, solid state, Raman, and parametric amplifiers which utilize different physical, electrical, and quantum properties of the light to create a gain [6]. The amplifier chain of the drive laser system at FAST is composed of diode-pumped solid state (DPSS) amplifiers which utilize the optical signals from laser diodes to produce amplification of the input laser light.

Diode End-Pumped Amplifiers

The goal of optical pumping is to excite the atoms in a gain medium into higher energy levels and eventually force a population inversion within the material. The creation of a population inversion will result in the stimulated emission of electromagnetic radiation in the form of photons which in turn amplifies the overall energy of the seed laser beam.

End pumping in particular utilizes the principles of optical pumping by injecting light along the same path as the laser beam being amplified. This method of amplification is beneficial because it

provides higher quality beams and power efficiency [7]. However, end pumping is limited because the pump light can only be injected from two directions at most. In contrast, side pumping allows for light to excite the gain medium from nearly any direction. Side pumping is not as effective as end pumping because it does not interact as accurately or intensely with the gain medium, causing less amplification to be attained.

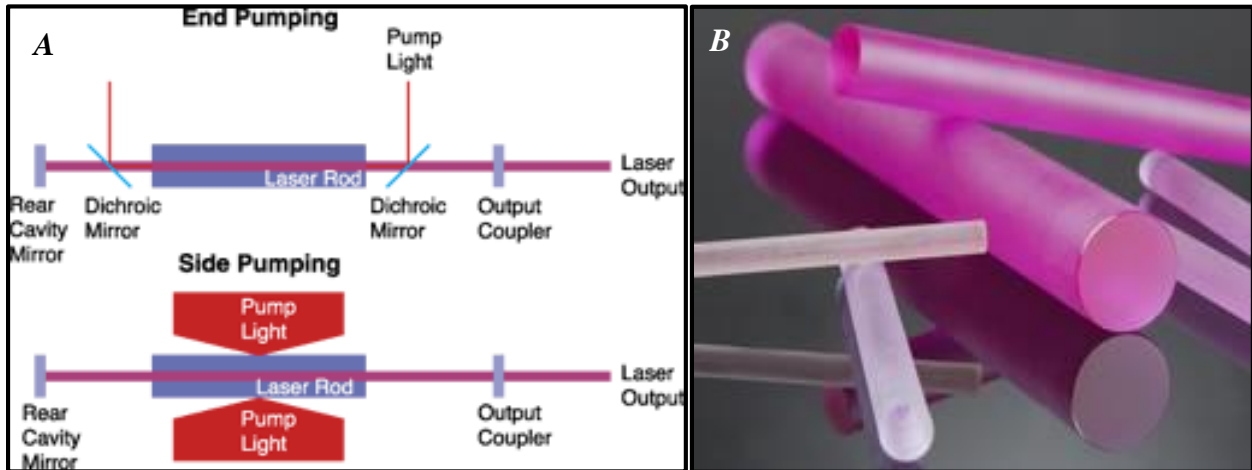


Figure 5. A) Schematic diagram depicting the design differences between end-pumped and side-pumped amplifiers. Adopted from [28]. B) Neodymium-doped yttrium-lithium fluoride (Nd:YLF) crystals of various lengths and diameters. Adopted from [29].

Nd:YLF as a Gain Medium

The choice of gain medium for an optical amplifier is significant because it has the ability to considerably limit the gain, or amount of amplification, produced by the system. Gain media come in various forms including semiconductors, laser crystals and glasses, ceramics, and laser dyes, with laser crystals being one of the most widely-used [8]. The laser crystals used as gain media are typically doped with laser-active ions such as rare-earth or transition metals.

The Nd:YLF crystal used as the gain medium in each of the three pre-amplifiers and the three single-pass solid-state amplifiers mainly consists of yttrium-lithium fluoride (LiYF_4), abbreviate to YLF, doped with an optimal amount of the rare-earth metal, neodymium (Nd). A key characteristic of the Nd:YLF crystal is its natural birefringence, or polarization-dependent index of refraction. Depending on the polarization of the incoming light, one of two laser transitions will be activated. A strong transition at 1047 nm is present when π -polarized light is present, and a weaker 1053 nm transition is activated by σ -polarized light [9].

Nd:YLF Energy Levels and Transitions

The amplifiers of the FAST drive laser system are an example of a four-level laser system. The counter-propagating 808 nm diode pulses excite the electrons of the dopant neodymium atoms substituted in the crystal lattice of yttrium-lithium fluoride from the $^4\text{I}_{9/2}$ state to the $^4\text{F}_{5/2}$ state. Via a non-radiative transition process, the electrons settle into the metastable $^4\text{F}_{3/2}$ energy level with a longer lifetime. As the seed pulses of 1053 nm light pass through the Nd:YLF crystals, an energy level transition is triggered from the $^4\text{F}_{3/2}$ state to the $^4\text{I}_{11/2}$ state, which is continued by a chain reaction of stimulated emission by the seed pulses.

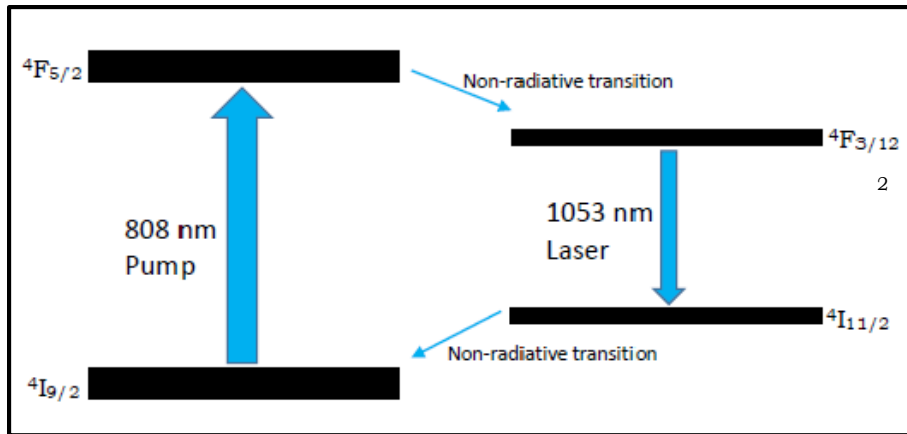


Figure 6. The energy level transitions of the four-level Nd:YLF amplifier chain of the drive laser system at FAST. Adapted from [24].

Electron Bunches

The successful operation of the superconducting test accelerator at FAST relies on the generation of electron bunches in the 1- $\frac{1}{2}$ cell 1.3 GHz electron gun, of the same design used at the Photo Injector Test Facility (PITZ) at DESY Zeuthen [10]. The gun contains a photocathode which consists of a 5 mm diameter photosensitive area that, when struck with electromagnetic radiation, emits bunches of high energy electrons that are accelerated, steered, and focused further downstream in the beamline in superconducting RF cavities and magnetic fields.

The Photoelectric Effect

In the late 1800s, there was much debate among physicists about the nature of light. Although experimental evidence of light behaving as waves had already been found, the observations of Heinrich Hertz and Philipp Lenard puzzled the community. They found that as light struck a metal surface of sodium, electrons of a specific energy were emitted. Hertz and Lenard noticed that not all wavelengths of light were able to induce electron emission from the metal. For instance, a red beam of light, no matter the intensity, did not produce electrons. The higher the frequency of the incident light, the higher the kinetic energy of the emitted electrons. The results from these

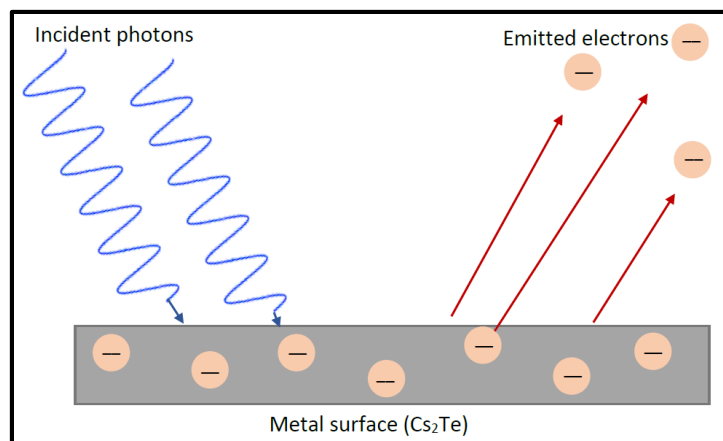


Figure 7. A schematic drawing showing high-energy photons striking a Cs₂Te surface and ejecting electrons from the atoms in the metal by the photoelectric effect.

experiments were characteristic of a light particle interacting with the metal rather than a light wave [11].

It was not until 1905 that Einstein's Nobel Prize-winning work explained the phenomena observed by Hertz and Lenard. The most prevalent trend in the early data followed that the energy of ejected electrons was proportional to the frequency of the incident light. With this in mind, Einstein postulated that light could also behave as discrete particles, or quanta, and that the energy and frequency of these light particles could be related by the equation

$$K_{max} = h(f - f_0) \quad [1]$$

in which K_{max} is the maximum kinetic energy of the ejected electrons, h is Planck's constant, f is the frequency of the incident light, and f_0 is the threshold frequency of the metal surface [12]. The same equation can also be written in terms of the energy of the absorbed photons and the work function of the surface, ϕ [11].

$$K_{max} = E - \phi \quad [2]$$

Both of these equations can be simplified to the most basic description of the electromagnetic spectrum

$$E = hv = \frac{hc}{\lambda} \quad [3]$$

Robert Millikan's 1916 paper which detailed his determination of Planck's constant h by the photoelectric effect, proved Einstein's theory of the particle nature of light. Millikan found a value of $h = 6.57 \times 10^{-27}$ erg-seconds = 6.57×10^{-34} Js [13]. Einstein's theory and Millikan's experimental evidence gave rise to the wave-particle duality of light.

Photocathodes

Photocathodes are the most promising source of electrons used in high-energy physics accelerator technology. They have become especially popular as superconducting radiofrequency (SRF) cavity technology has continued to develop and become more widely used. The technology and engineering of photocathodes is continuously developing, and photocathodes can now be made from metals, semiconductors, and superconducting material [14].

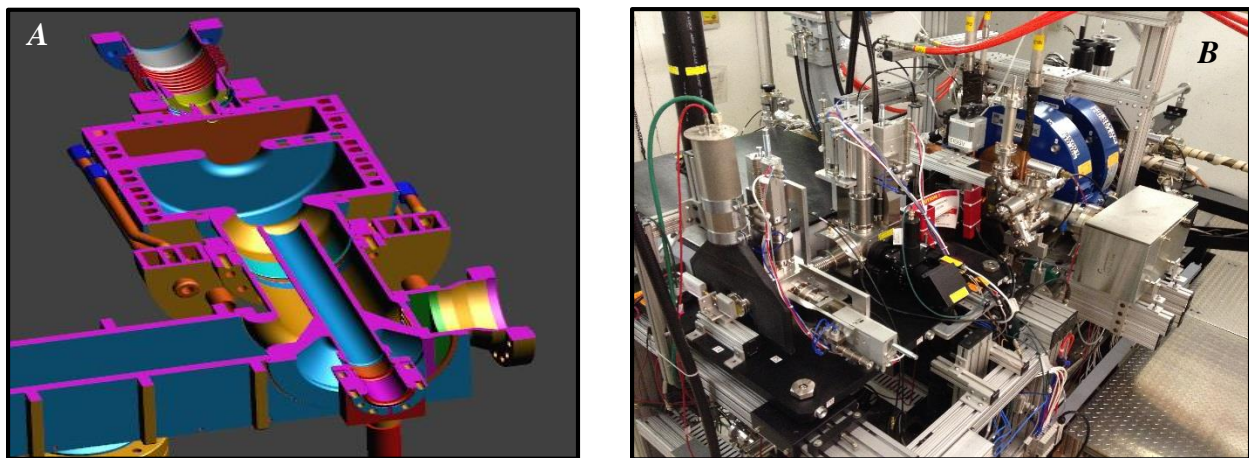


Figure 8. A) A 3D cross-section of the engineer drawing of the RF electron gun based on the PITZ design at DESY Zeuthen. B) A photograph of the electron gun at the upstream end of the beamline enclosure at FAST.

The photocathode in the photoinjector at FAST consists of a 10 mm diameter molybdenum disk containing a central photosensitive area coated with Cs₂Te [1]. The photocathode is an example of a semiconductor cathode. Cs₂Te is a p-type semiconductor with a band gap of 3.2 eV and an electron affinity of 0.3 eV, requiring the incident laser light to have a wavelength in the ultraviolet region [14]. This alkali antimonide also has relatively high quantum efficiency (10%-1%) over a relatively long period of time and can be rejuvenated after its efficiency drops, making it the most effective choice of material for the photocathode in the RF gun at FAST [15].

SIST Project Description

The goal of this summer project through Fermilab's Summer Internships in Science and Technology (SIST) program was to increase the total amplification of the 1053 nm seed beam in the drive laser system at FAST Facility. In order to improve the amplifier chain, a test single-pass diode-pumped solid state amplifier was set up on a spare optics table in the laser lab used for laser R&D experiments. Sending seed pulses to the test amplifier from the output of SPA1, the amplifier was optimized with a series of realignments, adjustments of optical components and diode timing parameters, and beam spot analyses. After maximizing the gain from the test amplifier, it would replace the current SPA3 on the main optics table in order for the drive laser system to operate more effectively.

Methods

Instrumentation

Laser Probe Inc. Rm-3700 Universal Radiometer

Energy measurements of the pulse trains were taken using the Laser Probe Inc. Rm-3700 series Universal Radiometer. The radiometer parameters allowed for averaging the energy of externally triggered pulses with a sensitivity ranging from 0.10 μJ to 100.0 J [16]. The radiometer has an accuracy of 0.5% and can be connected to different probes depending on the desired sensitivity and range of measurements.

Thorlabs DET10A Si Biased Detector

The Thorlabs DET10A is a silicon-biased detector sensitive to optical signals between 200 nm and 1100 nm [17]. The photodiode operates with a high quantum efficiency and generates a current when light is absorbed. The detector is equipped with an optical coupler which allows for addition of optical density filters. The output signal of the detector was connected to the Agilent oscilloscope for signal readout.

Agilent Technologies DSO6104A Digital Storage Oscilloscope

The readout from the Thorlabs DET10A detector was connected to the Agilent Technologies DSO6104A Digital Storage Oscilloscope. The light signals from the laser pulses were converted to voltages for display on the front panel. The oscilloscope has a 1 GHz bandwidth and 4 analog channels with a sampling speed of 4 GSa/s [18].

Prosilica GC 2450 CCD Camera

In order to characterize the profile of the seed beam, the Prosilica GC 2450 CCD camera was used to capture images of the infrared pulses. The camera has a resolution of 2448 x 2050 and a pixel calibration size of 3.45 μm [19]. An optical coupler can be added to the camera for the connection of filters to protect the sensor from high-intensity optical signals and burns. The images were monitored and captured using the Accelerator Controls Department (ACD) Java application, Image Tool [20].

Drive Laser System Schematic

The drive laser system housed in the laser lab at FAST is responsible for the production of ultraviolet (UV) light pulses with enough energy to create electron bunches from the Cs_2Te photocathode of the RF electron gun. A YLF seed laser from Time-Bandwidth Products GE-100 Series is mode-locked to a harmonic of the 1.3 GHz master oscillator to produce the infrared (IR) seed beam at 81.25 MHz [21]. The oscillator creates a pulse train with a 3 ps RMS pulse width. While it is capable of producing up to 3000 pulses per train, the seed oscillator typically operates between 1 and 500 pulses [3]. Independent of the number of pulses in a train, the 1053 nm pulses are spaced 333 ns (3 MHz) apart for a pulse train width of 1 ms with a repetition rate of 5 Hz [3].

Seven stages of amplification increase the 1053 nm seed beam energy for higher ultraviolet pulse energies and effective electron emission in the photocathode. The chain is broken into three phases: pre-amplifiers, single-pass amplifiers, and a commercial amplifier made by Northrop Grumman,

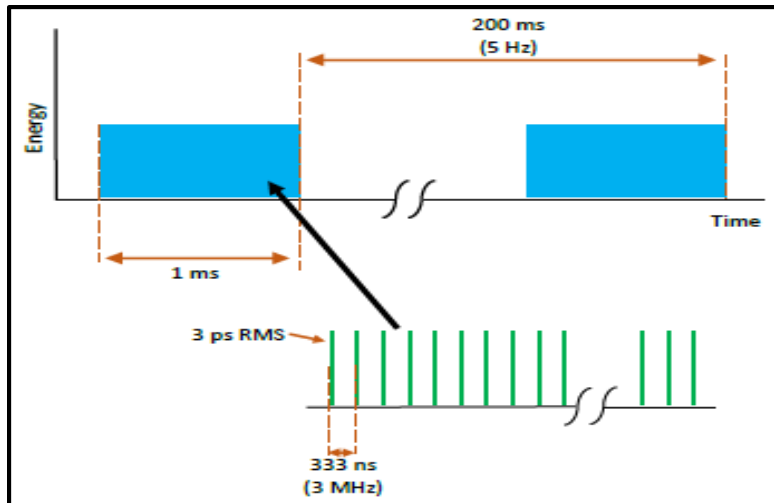


Figure 9. The time structure of the FAST laser beam, showing the individual pulses that make up each 1 ms long pulse train and their repetition rates. Adapted from [2].

each of which is staged on its own 12" x 12" breadboard. The three pre-amplifiers output pulses with energies of $\sim 1 \mu\text{J}$. Before entering the next stage of amplification, the seed beam passes through a Pockels Cell (PC1), or pulse cleaner, which allows for precise control of the timing of the output light. The three single-pass amplifiers (SPA1-3) provide the drive laser with more gain than the pre-amplifiers, with initial design specifications reaching an energy output of $15 \mu\text{J}$ per pulse at the end of the SPA chain. A second Pockels cell is located between SPA2 and SPA3 for further pulse cleaning. The Northrop Grumman amplifier (NGA) is also a single-pass amplifier and is responsible for the greatest amplification in the drive laser system. According to the initial drive laser design, NGA should emit pulse trains with energies of $\sim 50 \mu\text{J}$ per pulse [3].

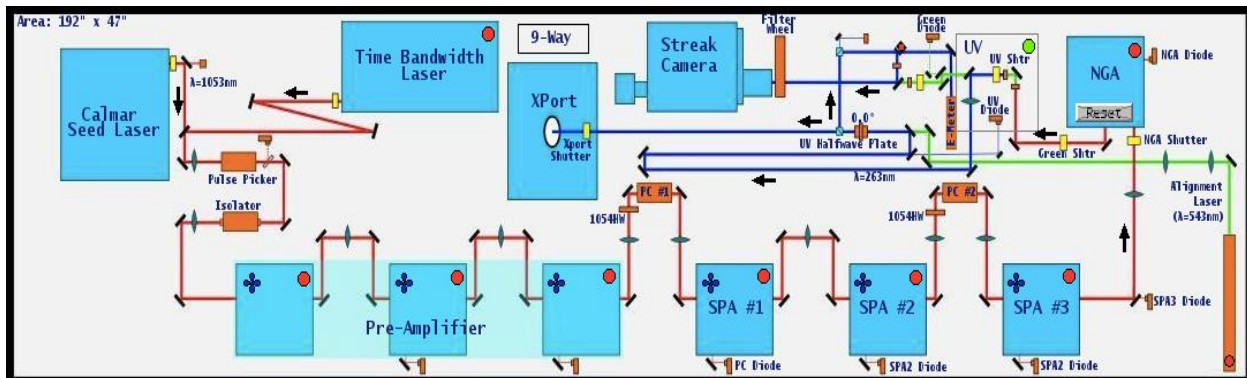


Figure 10. A diagram of the main optics table in the FAST laser lab and the beam path through the drive laser system. Taken from the ACNET console.

Seed Pulse Pick-Off

During early work on the test single-pass amplifier (SPAT), seed beam had to be taken from the main optics table and propagated across one of the walkways to the sandbox optics table where the SPAT breadboard was stationed. Initially, the seed was picked off with a flipper mirror directly after SPA1, however this prevented any seed from reaching the rest of the laser system and, therefore, the photocathode. Without UV photons bombarding the photocathode, no electron

bunches can be produced, preventing electron beam from running in the enclosure. This significantly limits the time when diagnostic work can be done on the 1053 nm seed pulses.

A new method of delivering seed beam to the sandbox table parasitically was conceived, utilizing the leakage of mixed green and infrared laser light inside the ultraviolet box. This leftover light is a result of the small amount of beam that is transmitted, rather than reflected, through the mirror downstream of the first frequency-doubling crystal. By adding a prism intercepting the leakage from the dielectric mirror at the correct angle and orientation, the infrared light can be separated from the green. Enough separation allows the IR light to pass through a hole in the side of the ultraviolet box, while the more dangerous green light is sent to a beam dump within the protective box. This new operating procedure will allow for more efficient laser R&D work to be completed without interrupting electron beam operation in the future.

Nd:YLF Amplifier Schematic

Each of the three pre-amplifiers and three single-pass amplifiers are configured in the same optical design. The input seed beam is directed toward the Nd:YLF crystal using a series of mirrors and passes through a half-wave plate ($\lambda/2$) to optimize the transmission of light with the desired polarization (σ -polarization) through the laser crystal. The manipulation of the polarization is essential for obtaining the maximum gain from the last two stages of amplification due to the birefringent nature of Nd:YLF. On the sandbox table, the seed beam was focused using a +300 mm lens through the center of the 4 mm diameter crystal. Concurrently, diode fibers in the near infrared region were focused through +75 mm lenses on either end of the crystal. Using two dielectric mirrors, the diode pulses are counter-propagated through the gain medium, activating the electrons of the dopant neodymium atoms to a higher energy level, from which the 1053 nm seed pulse trains obtain amplification via stimulated emission.

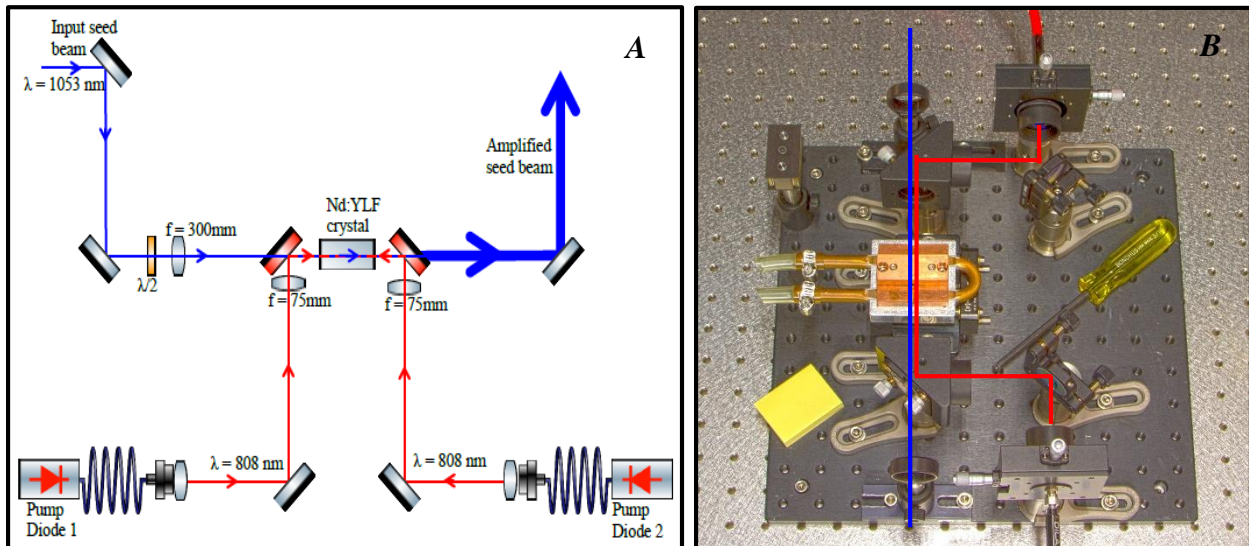


Figure 11. A) Diode-pumped solid state (DPSS) amplifier design, which each of the pre-amplifiers and single-pass amplifiers has. B) One of the amplifiers from the drive laser system showing the beam paths through the various optics. Red is the pump diode path and blue is the seed beam path.

Data and Results

Preliminary Measurements

Before beginning work to optimize the drive laser's amplifier chain, a series of preliminary measurements were made to characterize the initial effectiveness of the amplifiers and the relevant properties of the lasers used. Both single-pass amplifier 3 (SPA3) and the spare amplifier that replaced it, the test single-pass amplifier (SPAT), were analyzed before any optical adjustments or design changes were made.

Pump Diode Characterization

In each single-pass amplifier in the chain on the main optics table, the Nd:YLF crystal is end-pumped by two laser diode fibers which emit 808 nm light pulses. An extra pair of these diodes and their corresponding power system was also used on the sandbox table to pump SPAT during optimization of the design and alignment.

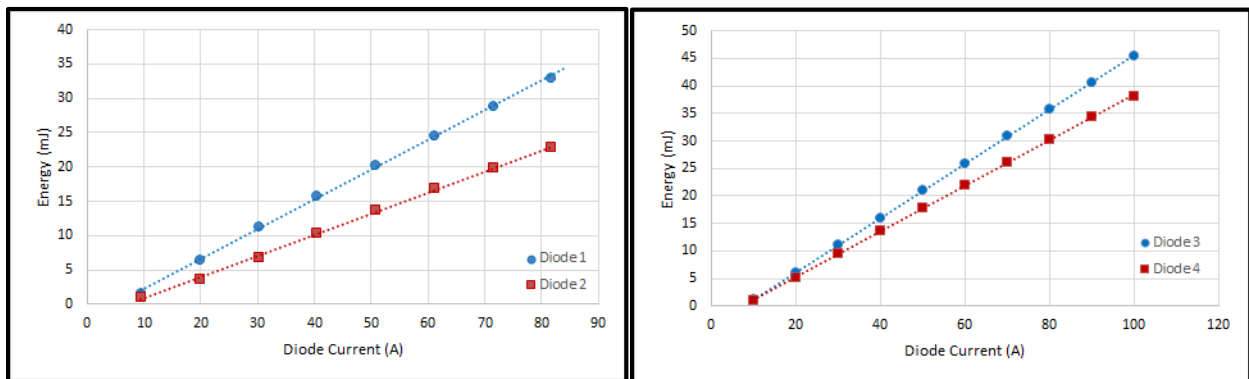


Figure 12. A) Comparisons of the diodes which pumped SPA3 on the main optics table and SPAT on the sandbox optics table during measurements and testing.

The energy of the light emitted from the diodes pumping SPA3 and SPAT were measured with varying currents from 10 A to 100 A. Both sets of diodes exhibited some disparity in the output energies as the current was increased. The diodes on the main optics table pumping SPA3 showed a maximum difference in energy of 10.2 mJ at 81.8 A. Diode 1 (S/N 6288), on the east side of the SPA3 breadboard, had higher pulse energy outputs than Diode 2 (S/N 6301). The diodes on the sandbox table only differed by, at most, 7.4 mJ at a maximum pump current of 100 A. Although this difference was not as significant as that found in the SPA3 diodes, the pulses from Diode 4 (S/N 901323) displayed a slight doughnut structure on the infrared detection cards used to align the beams through the amplifier optics. In comparison to the pulse shape of Diode 3 (S/N 901326), which was circular and showed equally distributed irradiance, the pulses from Diode 4 were clearly weaker in the center than on the outer edge of the circular beam spot. The observation of diode energy differences was taken into account while completing alignments with both sets of diodes.

Single-Pass Amplifier 3 (SPA3)

Before being replaced with SPAT, preliminary energy measurements were taken of SPA3 to determine the gain being obtained by the initial alignment of the amplifier under normal laser

system operation parameters. Changing the number of seed pulses in each train, an input and output energy reading was taken to determine the gain. The input energies were measured just after the seed beam passed through Pockels cell 2 (PC2) and the output measurements were taken before the seed entered the Northrop Grumman Amplifier (NGA) box.

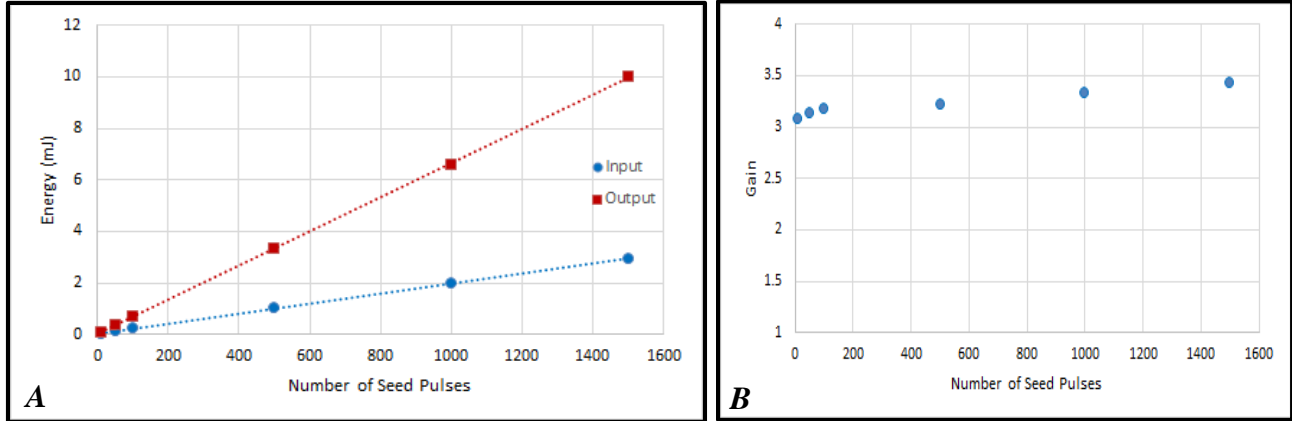


Figure 13. A) Plot of the input and output energies of SPA3 at various numbers of seed pulses. B) The corresponding gains of each of the measurements taken as a function of the number of pulses per train.

Given the input energy, E_i , and the output energy, E_o , the gain of each set of measurements can be calculated using the formula

$$g = \frac{E_i}{E_o} \quad [4]$$

resulting in an average gain of 3.23. A slight trend in the calculated gain value was observed as the number of seed pulses was increased. In a pulse train of 10 seed pulses, the gain was found to be 3.08. At the upper end of the data points, with 1500 pulses per train, the gain increased to 3.43. At the typical operating parameter of 50 pulses per train, the gain achieved by SPA3 was 3.14.

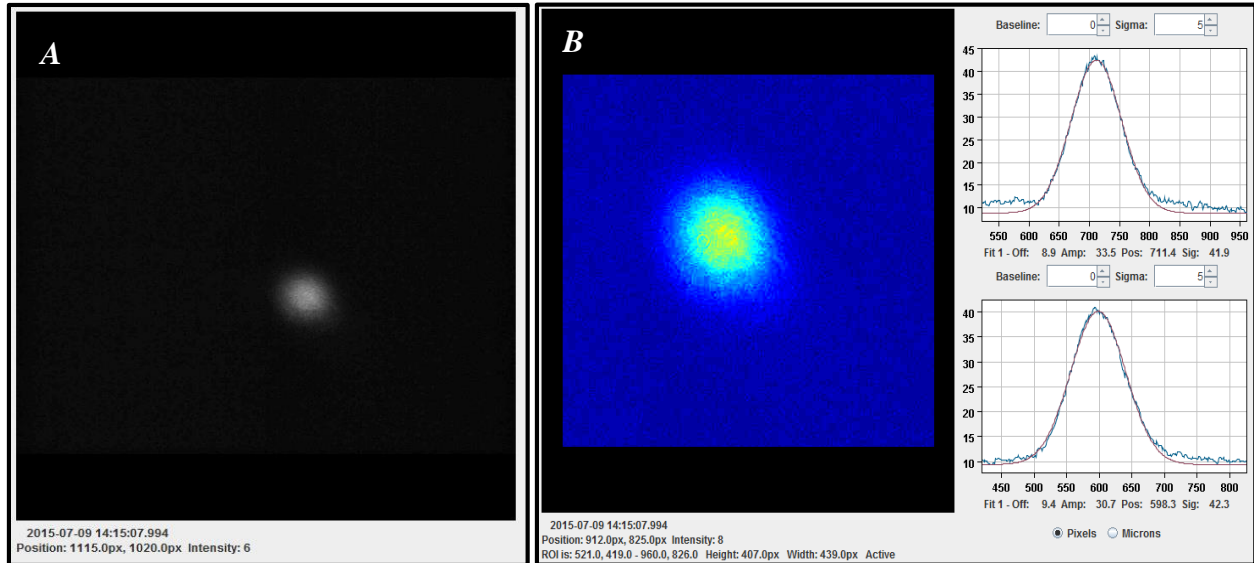


Figure 14. A). Beam spot image of SPA3 seed beam at crystal distance. B) Zoomed in, pseudo-color image of the SPA3 crystal distance beam spot with graphs plotting the Gaussian fit.

A spot size analysis was completed of the seed beam before it entered SPA3. The measurements were taken after the +300 mm focusing lens at crystal distance to analyze the beam spot at its focal point within the crystal. Using a Prosilica CCD camera and Image Tool, the laser pulse was found to have an approximately Gaussian profile. The plot fitting tool found the sigma values of the beam image to be about 42 pixels, corresponding to a sigma along the horizontal axis of 144.5 μm and 145.9 μm along the vertical axis.

Test Single-Pass Amplifier (SPAT)

Before beginning alignment and design adjustments on SPAT, it was necessary to obtain a baseline gain measurement of the amplifier. Only a rough alignment was made of the seed beam through SPAT at first because the beam had to be propagated across the walkway between the main optics table and the sandbox table to even reach the amplifier before any further alignments could be made. With the seed passing through the Nd:YLF crystal, the pump diode current was increased in steps of ten from 0 A to 100 A while energy of the seed beam of 50 pulses per pulse train was measured after being amplified. The calculated gain was only 1.79 for the initial alignment through SPAT at 100 A.

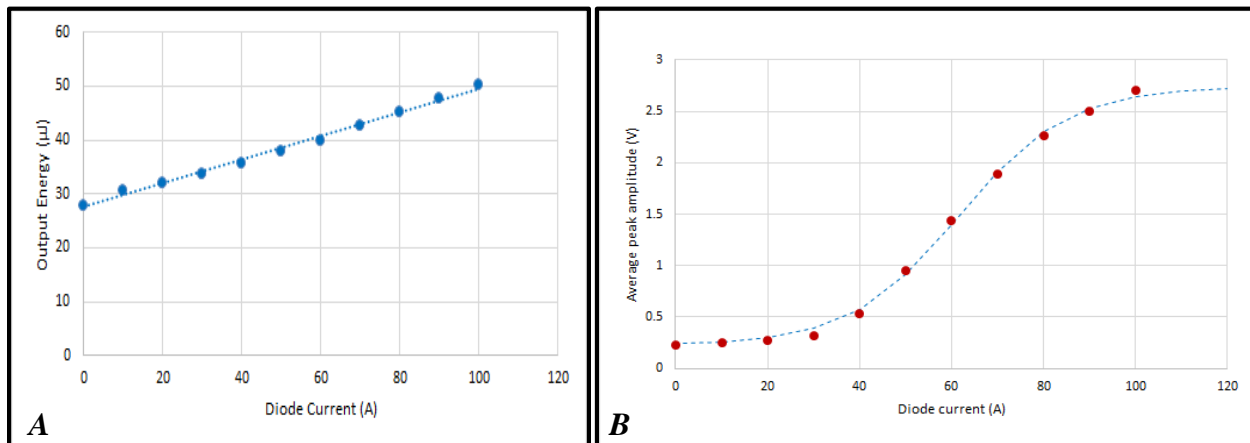


Figure 15. *A) Linear trend in the gain from SPAT as diode current was increased. B) Sigmoid curve trend of the voltage of the seed pulse signals through SPAT as it is pumped with larger currents.*

The gain profile of SPAT was also measured and plotted using a photodiode connected to the Agilent oscilloscope which output the voltage equivalent to the optical signal of the laser pulses. The voltage measurements were taken in the same manner as the initial energy measurements. When plotted, the voltage increases following a sigmoid curve which shows the increasing saturation of the gain medium as it is pumped by increasing diode current. When the current reaches 40 A, the slope of the curve increases, showing greater amplification of the seed beam. As the Nd:YLF crystal approaches saturation (~90-100 A) the slope begins to flatten out and the amplification factor is not as significantly increased as the diode current is increased.

The beam spot analysis of the seed beam at the sandbox table prior to passing through SPAT showed a beam profile smaller than the beam at crystal distance of SPA3 on the main optics table. The horizontal sigma was 33.4 pixels or 115.2 μm , and the vertical sigma was 32.0 pixels or 110.4 μm . The sigma values of the SPAT pulses were approximately 30 microns smaller than those of the SPA3 beam. Although the image capture shows a slightly skewed beam profile, the rippled

pattern on the top right edge of the beam spot is accounted for by the diffraction off of a dust particle on the camera's lens.

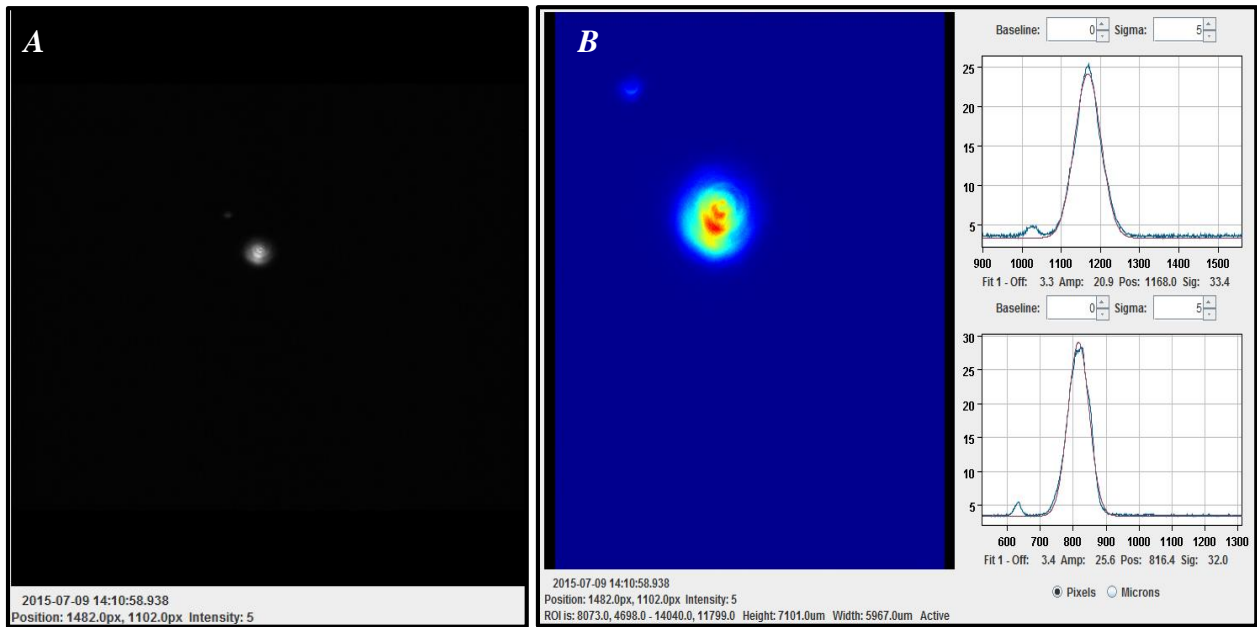


Figure 16. A) Beam spot image of SPAT seed beam at crystal distance. B) Zoomed in, pseudo-color image of the SPAT crystal distance beam spot with graphs plotting the Gaussian fit.

Timing Adjustments

Aside from improving the overall gain of the amplifier chain, achieving flat pulse trains is a key focus for the most efficient and optimized operation of the drive laser system at FAST. By adjusting the timing of the pump diodes' trigger delays and pulse width, the 808 nm diode pulses can be better synchronized with the 1053 nm seed pulses. This allows for more effective amplifier



Figure 17. A) Pulse train oscilloscope output without timing adjustments, showing a negative slope. B) Pulse train oscilloscope output after pump diode timing adjustments were made, showing the desired flat pulse train for 2000 pulses per train.

operation and flattened pulse trains, resulting in more consistent electron bunch production from the photocathode for use by the experimenters.

Although the drive laser is only typically operated with 50 pulses per bunch, the seed laser is capable of creating pulse trains of up to 3000 pulses. Adjustments were made to the pump diode timing parameters to optimize the pulse shapes for trains of 20 to 2000 seed pulses. The SPAT pump diode trigger delay and pulse width were changed to eliminate the negative slope of a train of 2000 seed pulses and achieve a flattened peak. The delay was increased from 1.097 ms to 1.718 ms, and the width was shorted from 1.856 ms to 1.280 ms. These corrected parameters provided consistently flat peaks for all shorter pulse trains and allowed for improved amplification factors with alignment corrections.

Alignment Work

In order to optimize the gain through SPAT, a series of adjustments to the beam alignment, beam size, and timing parameters had to be made. Slight changes were made to the optical design on the sandbox table, including the addition of a half-wave plate and the switching out of focusing lenses with different focal lengths. With each change made to the optics of the system, precise alignment of the seed beam and pump diode pulses had to be achieved. Better amplification was achieved when the seed pulse was focused through the middle of the Nd:YLF crystal and when the seed beam was slightly smaller in diameter than the pump diode pulses so that the entire 1053 nm pulse was being amplified by the excited electrons in the gain medium.

Maximization of SPAT Amplification

After multiple iterations of realignment, timing adjustments, and beam spot analyses, the amplification factor of SPAT was significantly improved. Measurements were taken of the seed beam power through the amplifier on the sandbox table with 0 A and 90 A of diode current. With 50 seed pulses per train, a gain of 8.60 was achieved from SPAT, which was more than twice the gain of SPA3 with the same number of seed pulses being amplified.

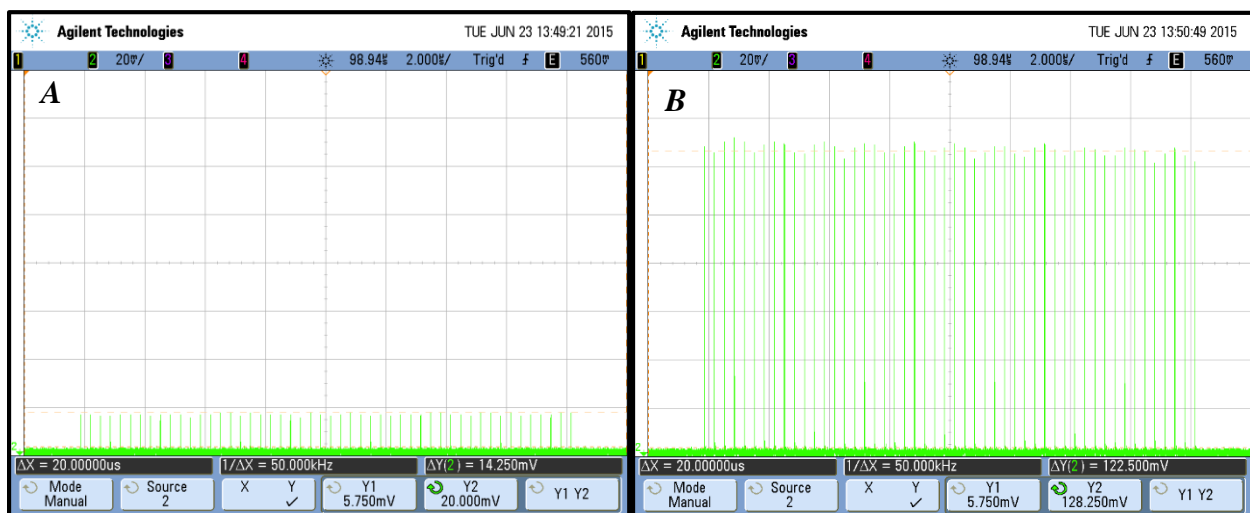


Figure 18. A) Oscilloscope output through SPAT with 0 A of diode current, with an average amplitude of 14.25 mV. B) Oscilloscope output through SPAT with 90 A of diode current, with an average amplitude of 122.50 mV.

After several more precise realignments were performed, energy measurements were also taken to determine the maximized gain through SPAT on the sandbox table. With 50 seed pulses per bunch, the energy with 0 A of diode current pumping the Nd:YLF crystal was 10.2 μJ , equivalent to 0.204 μJ per pulse. With a 90 A diode current, the measured energy was 107.9 μJ , or 2.158 μJ per pulse. These measurements correspond to a gain of 10.58 from SPAT.

Switching SPAT and SPA3

With the gain of 10.58 attained through SPAT on the sandbox table, the SPA3 breadboard was removed from the main optics table and replaced with SPAT. Because so many optical components were replaced, all elements downstream of the new SPA3 had to be realigned through the existing optics of the Northrop Grumman Amplifier (NGA) and the frequency-doubling crystals in the UV box.

As expected, the gain achieved on the sandbox table through SPAT was reduced due to the amplified energy of the seed beam from SPA2 and the pulse cleaning through PC2 when introduced on the main optics table. Using the energy meter to measure the input and output seed energy of the new SPA3, the gain was found to be 4.83.

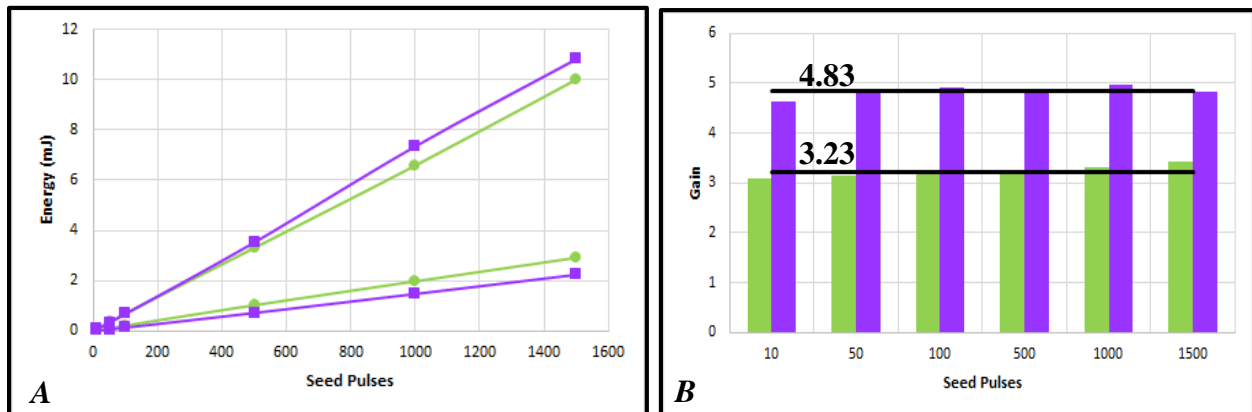


Figure 19. *A) Comparison plot of the old SPA3 (green) with the new SPA3 (purple). B) Gain comparison of the old SPA3 (average gain = 3.23) and the new SPA3 (average gain = 4.83) as a function of the number of pulses per train.*

Comparing the gain measurements obtained from the old SPA3 and the new SPA3 as a function of the number of seed pulses per pulse train shows the stability of the gain attained from the single-pass amplifiers in the chain. A relatively consistent trend in the gain can be seen no matter how many seed pulses are contained in the train. The increase from 3.23 to 4.83 is only an improvement of 1.5, and although this considerably lower than the results measured on the sandbox table, the amplification is still great enough to improve the ultraviolet pulse energy downstream.

Diagnostic Photodiode Calibration

Each amplifier in the seven stage chain is monitored via a photodiode which measures the seed beam leakage from the dielectric mirrors used in the optical design which are not 100% reflective for 1053 nm light. After introducing SPAT in place of SPA3, the diagnostic photodiodes for SPA2 and SPA3 had to be recalibrated.

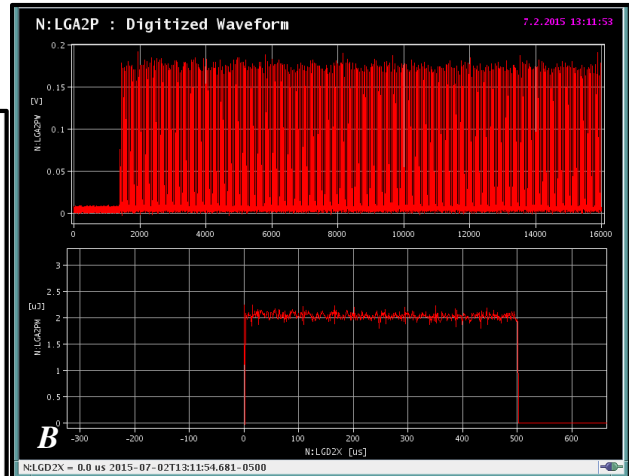
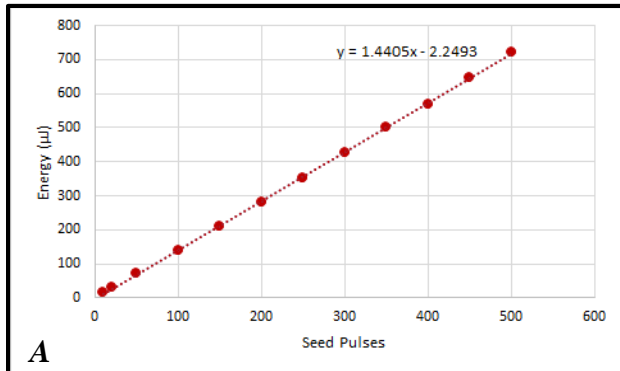


Figure 20. A) Calibration plot for the SPA2 diagnostic photodiode. B) Real-time measurements of the energy per pulse from the SPA2 diagnostic photodiode with 500 pulses per train.

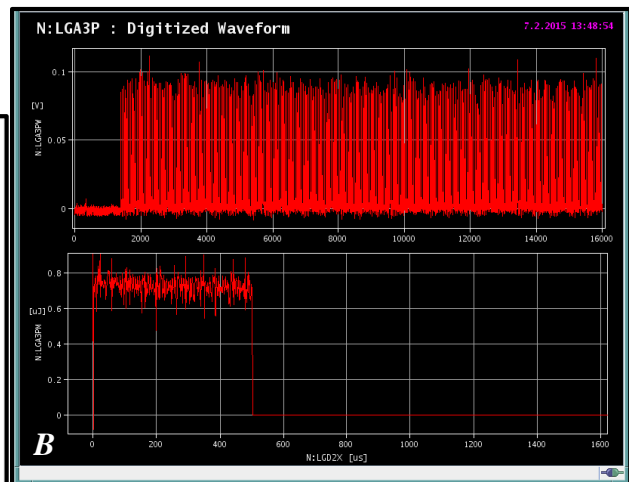
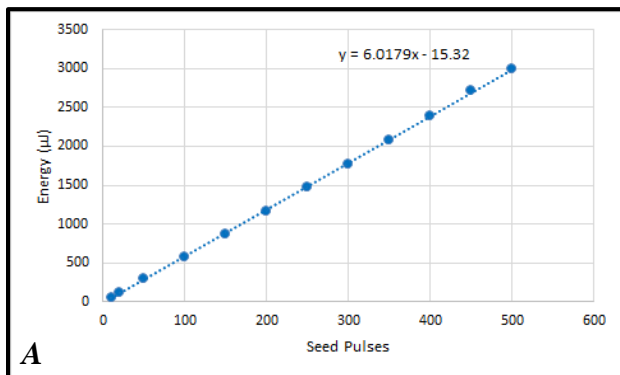


Figure 21. A) Calibration plot for the SPA3 diagnostic photodiode. B) Real-time measurements of the energy per pulse from the SPA3 diagnostic photodiode with 500 pulses per train.

By making a calibration plot of the energy of the beam leakage against the number of seed pulses, a linear trendline is plotted, the slope of which is the corrected energy per pulse to which the diode must be calibrated. The corrected values were input in the photodiode script and the digitized waveforms were monitored to ensure accurate calibration.

Downstream Results of New Amplifier

Although replacing SPA3 with SPAT only resulted in a 1.5 times increase in the gain from the sixth stage of amplification in the drive laser system, the true effects of this switch can be seen downstream of the new amplifier.

Effects on Northrop Grumman Amplifier (NGA)

As a result of switching SPA3 and SPAT, the laser had to be realigned through the Northrop Grumman Amplifier (NGA). Due to its design, it is necessary for the seed beam to completely fill the 3 mm diameter Nd:YLF crystal for maximum gain. By adjusting the intermediate optics

between the new SPA3 and NGA and by optimizing seed beam transmission through the NGA crystal, a larger amplification factor was attained from NGA. Using the same method of timing adjustments as with SPAT, output flat pulse trains were attained from NGA for up to 1000 pulses per train.

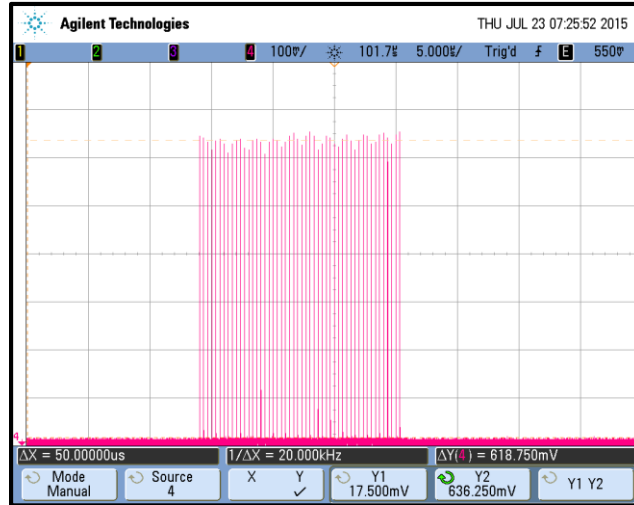


Figure 22. Oscilloscope readout of a pulse train amplified through NGA with a relatively stable amplitude and flattened peak.

Operating with 500 seed pulses per train, the IR beam had an input energy of 2.85 mJ (5.7 μ J per pulse) which was amplified to 32.4 mJ (64.8 μ J per pulse) through NGA pumped by 100 A of diode current. These energy measurements correspond to a gain of 11.37 from NGA, which has been improved by a factor of 1.5 from initial operation with the old SPA3. This amplification can be visualized from the CCD camera images of the seed beam through NGA with and without pumping. The ripple effect on the left edge of the beam spot is the result of diffraction off of burn spot on the camera lens.

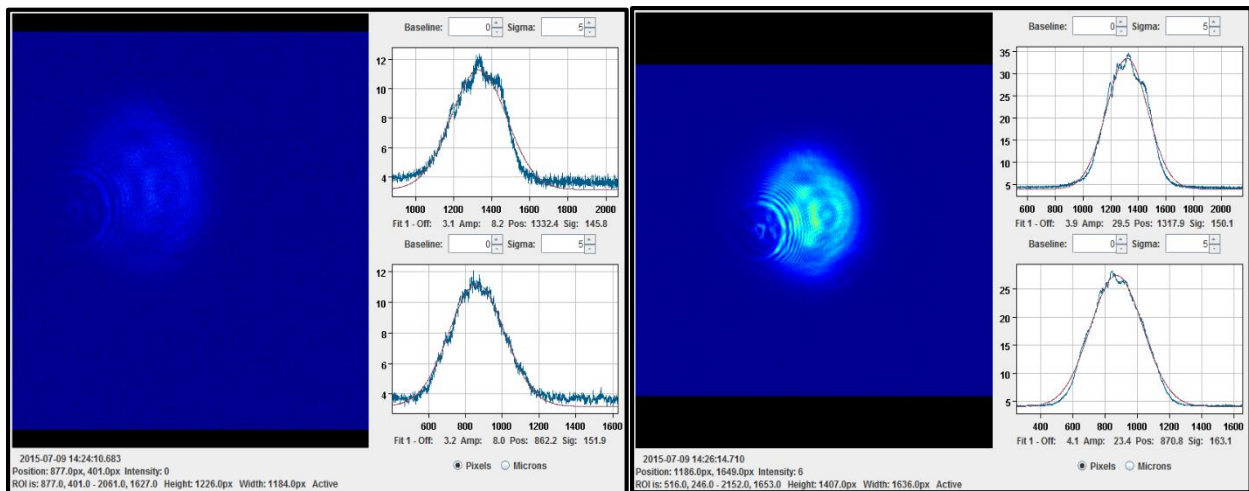


Figure 23. A) Pseudo-color beam spot image of the output from NGA with no pump diode current. B) Pseudo-color beam spot image of the output from NGA with 100 A of diode current.

Effects on Ultraviolet Pulse Energy

With the increase in energy per pulse from the new SPA3 and the subsequent NGA, the ultraviolet pulse energy was improved significantly. The BBO frequency-doubling crystals used to generate the UV light have, at maximum, a transmission efficiency of ~50%, a large amount of energy is lost in this section of the drive laser system. Before the new SPA3 was inserted in the amplifier chain, the energy of the UV beam transported to the RF electron gun was only ~4.5 $\mu\text{J}/\text{pulse}$. After optimizing alignment through the doubling crystals and downstream optical elements which send the beam to the transport line, the UV pulse energy has been increased to 10.2 $\mu\text{J}/\text{pulse}$. With a pulse train of 50 pulses per bunch, the energy meter measured 511 μJ , an ultraviolet pulse energy increase of 2.3.

Conclusions

The diode-pumped solid state (DPSS) amplifier chain for the 263 nm drive laser system at FAST Facility has been improved by the addition of a new, optimized amplifier in place of SPA3. The test amplifier produced a gain of 10.58 during alignment work on the spare optics table before being installed on the main optics table. After installation was completed, a gain of 4.83 was attained from the new amplifier due to higher input energies and pulse cleaning through a Pockels cell.

Downstream of the new amplifier, the Northrop Grumman amplifier's gain was increased to 11.37 with pulse energies of approximately 65 μJ per pulse. Through pump diode timing adjustments, the amplified output pulse trains from the new SPA3 and NGA were attained for consistent ejection of electrons from the photocathode in the beamline's electron gun.

The energy of the ultraviolet pulses was more than doubled, resulting in energies of 10.2 μJ per pulse being transported through from the laser lab to the beam enclosure for imaging onto the Cs_2Te photocathode. This increase in energy will provide more electron bunches to be emitted from the photocathode during electron beam operation.

Future Work

Once the installation of the new amplifier in the drive laser system was completed, final measurements were taken of each of the single-pass amplifier stages, NGA, and through the frequency-doubling crystals. SPA2 was found to only be producing a gain of 1.4 and will require improvement. With the old SPA3 now free to be tested and optimized, the same process will be repeated. The gain of the old SPA3 will be maximized through a series of precise realignments, optical component changes, and beam spot analyses. The properly tuned amplifier will then be used to replace SPA2 in the drive laser's amplifier chain, in hopes of increasing the gain in comparison to the current device.

The long term goal for improvement of the drive laser system at FAST is to attain a UV pulse energy of $\sim 50 \mu\text{J}$ per pulse. This will require optimization of the entire amplifier chain and drive laser system. With the timing adjustments made to attain flat pulse trains, the laser will begin to be operated with more pulses in each pulse train until the maximum 3000 pulses per train is reached.

Acknowledgements

I have had the most amazing time here at Fermilab this summer, meeting new people and learning new physics. Countless individuals have helped to make this experience one of the most rewarding of my undergraduate career. I would like to express my most sincere and heartfelt thanks to my supervisor, Jamie Santucci, for his enthusiasm, guidance, and eagerness to teach at every opportunity throughout the summer. I have learned so much from his extraordinary example in the past twelve weeks that will stay with me for the rest of my life. I would also like to thank Jinhao Ruan and Chip Edstrom for their expertise and mentorship as I learned about the laser system and completed work on my project. I want to thank the entire injectors group at FAST Facility, who I have been fortunate enough to get to know and work with this summer, for being so welcoming and willing to answer my questions. A special thanks goes out to Dan Broemmelsiek, Darren Crawford, Kermit Carlson, Wayne Johnson, Ron Kellet, Alex Lumpkin and Arden Warner. I would also like to thank the entire FAST/IOTA group for their support and kindness this summer.

I would like to thank my SIST mentor, Mayling Wong-Squires, for her guidance throughout the program. I sincerely thank the entire SIST Committee: Sandra Charles, Linda Diepholz, Dianne Engram, Gustavo Canselo, Bill Freeman, Elliott McCrory, Vivian O'Dell, and David Peterson, for giving me the opportunity to take part in this program. I also want to thank all of the SIST and GEM interns, especially my housemates, for such an amazing summer.

I would like to thank all of my professors and mentors at Duquesne University, particularly Dr. Simonetta Frittelli and Dr. Derrick Hilger, for their guidance during the application process. An extra special thanks goes out to my research advisor, Dr. Theodore Corcovilos, for taking a chance on me two years ago and, in doing so, helping me recognize my abilities and providing me with a diverse arsenal of laboratory and research skills, which have prepared me for this opportunity and those still to come.

Finally, none of this would have been possible without the constant love and support of my family. They have been my rock every step of the way as I pursue a future in physics and there are not enough words to express my gratefulness to them.

References

1. K. Carlson, et al., Fermi National Accelerator Laboratory. Design of the Advanced Superconducting Test Accelerator. Beams-doc-4212, 2012.
2. P.H. Garbincius, et al. Fermi National Accelerator Laboratory. Proposal for an Accelerator R&D User Facility at Fermilab's Advanced Superconducting Test Accelerator. Fermilab-TM-2568, 2013
3. J. Ruan. ASTA Injector Laser Lab Standard Operating Procedure, 2015
4. "Laser-based research and development at the CSIR: An overview." *Council for Scientific and Industrial Research*. 26 September 2007. Web.
http://www.csir.co.za/lasers/basics_of_lasers.html
5. "Introduction to Laser Technology – Basic Laser Principles." Melles Griot. 36.2-36.5
www.mellesgriot.com
6. Paschotta, Rudiger. "Optical Pumping." *RP Photonics Consulting GmbH*. Web.
http://www.rp-photonics.com/optical_pumping.html?s=ak
7. Paschotta, Rudiger. "End Pumping." *RP Photonics Consulting GmbH*. Web.
http://www.rp-photonics.com/end_pumping.html
8. Paschotta, Rudiger. "Gain Media." *RP Photonics Consulting GmbH*. Web.
http://www.rp-photonics.com/gain_media.html
9. Paschotta, Rudiger. "YLF Lasers." *RP Photonics Consulting GmbH*. Web.
http://www.rp-photonics.com/ylf_lasers.html?s=ak
10. "Photo Injector Test Facility at DESY, Location Zeuthen (PITZ) - Research and development." *Deutsches Elektronen-Synchrotron*. 2015. Web.
http://pitz.desy.de/research_and_development/
11. Elert, Glen. "Photoelectric Effect." *The Physics Hyper Textbook*. 2015. Web.
<http://physics.info/photoelectric/>
12. Aronst, A. B, and M. B. Peppard. "Einstein's Proposal of the Photon Concept – A Translation of the *Annalen der Physik* Paper of 1905." *American Journal of Physics* 33. 5 (1965): 367-374. Print.
13. Millikan, R. A. "A Direct Photoelectric Determination of Planck's 'h'." *Physical Review* 7. 3 (1916): 355-388. Print.
14. Xiang, R., A. Arnold, H. Buettig, D. Janssen, M. Justus, U. Lehnert, P. Michel, P. Murcek, A. Schamlott, Ch. Schneider, R. Schurig, F. Staugenbiel, and J. Teichert. "Cs₂Te

normal conducting photocathodes in the superconducting rf gun.” *Physical Review Special Topics – Accelerators and Beams* 13, 4 (2010): 1-7. Print.
DOI: 10.1103/PhysRevSTAB.13.043501

15. Loch, R. A. “Cesium-Telluride and Magnesium for high quality photocathodes - Preparation and diagnostics.” (Master thesis), University of Twente, The Netherlands. 2005.
16. “Rm-3700 Universal Radiometer.” Rev 0199801js. Laser Probe, Inc. 2001.
www.laserprobeinc.com
17. “DET10A(/M) Si Biased Detector User Guide.” Revision E. Thorlabs, Inc. 2015.
www.thorlabs.com
18. “Agilent 6000 Series Oscilloscope User’s Guide.” Fourth Edition. Agilent Technologies, Inc. 2006.
www.agilent.com
19. “Prosilica GC2450 Data Sheet.” Allied Vision Technologies. 2014.
<http://www.alliedvisiontec.com/us/products/cameras/gigabit-ethernet/prosilica-gc/gc2450.html>
20. “Image Tool” Accelerator Controls Department Java Application Index. Fermi National Accelerator Laboratory. 2015.
<http://www-bd.fnal.gov/appix/>
21. “GE-100 User Manual, Mode-Locked Diode-Pumped Picosecond Laser.” Version 2v4. Time-Bandwidth Products. 2005.
www.tbwp.com
22. “Fermilab’s Tevatron.” Fermi National Accelerator Laboratory. June 2012.
http://fnal.gov/pub/presspass/factsheets/pdfs/Tevatron_FactSheet_060612.pdf#page=1&zooom=auto,612,815
23. “About Fermi National Accelerator Laboratory.” Fermi National Accelerator Laboratory. April 2015.
http://fnal.gov/pub/presspass/factsheets/pdfs/AboutFermilab_FactSheet_040115.pdf
24. Bernhardt, E. H., C. Bollig, M. J. D. Esser, L. R. Botha, C. Jacobs. “A single-element plane-wave solid-state laser rate equation model.” *South African Journal of Science* 104, 9-10 (2008): 389-393.
25. “User Facilities Fermi Accelerator Complex.” U.S. Department of Energy, Office of Science. 2015.
<http://science.energy.gov/hep/facilities/user-facilities/fermilab-accelerator-complex/>

26. Valishev, A. "IOTA – A Brief Parametric Overview." 2015.
http://asta.fnal.gov/IOTA/IOTAmeeeting/IOTA_Short.pdf
27. "A Practical Guide to Lasers for Experimenters and Hobbyists." Sam's Laser FAQ. 2009.
<http://donklipstein.com/laserfaq.htm>
28. Keirstead, M. "Pump Up the Volume." SPIE. 2001.
DOI: 10.1117/2.5200111.0008
29. "Nd:YLF Laser Rods – An Alternative to Nd:YAG." Laser Components. 2010.
<http://www.lasercomponents.com/us/news/ndylf-laser-rods-an-alternative-to-ndyag/>
30. "Photo Gallery" Fermilab Visual Media Services.
<http://vms.fnal.gov/asset/photogallery>